Theor Chem Acc (2001) 105:284–291
DOI 10.1007/s002140000229

Theoretical
Chemistry Accounts

Regular article

Complementary aspects of charge and momentum density for the study of the chemical bond

Pierre J. Becker, Jean Michel Gillet, Pietro Cortona, Sebastien Ragot

Laboratoire SPMS, CNRS and Ecole Centrale Paris, Grande Voie des Vignes, 92295 Chatenay Malabry Cedex, France

Received: 19 July 2000 / Accepted: 11 October 2000 / Published online: 19 January 2001

Abstract. Charge density can be accessed through accurate X-ray diffraction by crystals. It has recently become a rather routine technique. Refinement models enable a fair description of charge density changes due to chemical bonding and cohesive forces. Conversely, momentum density is observable through incoherent Compton scattering, in particular by use of high-intensity synchrotron sources. We present results concerning a first attempt at a simultaneous refinement of a model wavefunction on both diffraction and Compton data, for MgO and LiH crystals. It is shown that if the diffraction data are highly sensitive to local effects and their symmetry around atomic sites, Compton data are very dependent on the delocalization processes of electrons. Moreover, Compton measurements show a systematic deviation from self-consistent-field model calculations and this is analyzed in terms of an empirical correlation model for anions in insulators. Possible future extensions of such studies are finally discussed.

Key words: Charge density – Momentum density – Compton scattering – Bragg scattering – Wavefunction refinement

1 Some aspects of Bragg scattering and charge density models

Charge density is an essential function for the understanding of chemical bonding. The development of density functional theory (DFT) led to the possibility for theoretical prediction of physical and chemical behavior of many realistic systems [1, 2]. The role of charge density is reinforced by the fact that it can be approached via X-ray Bragg diffraction by crystalline materials. Specific models exist that allow the electron density to be recovered from diffraction intensities [1]. Global results of such refinements are generally in good agreement with both self-consistent-field (SCF) and DFT calculations. Recent studies have thus been undertaken concerning complex structures (both mineral, such as zeolites, and organic, such as polypeptides) for which ab initio calculations at a quantitative level are still questionable [3, 4]. Pioneering experimental work has also been performed by Pressprich et al. [5] beyond the ground state in crystals exhibiting metastable excited states.

However, charge density models used in X-ray diffraction refinements are dictated by the optical nature of the scattering process. Let us just recall that the observed intensity is given by

$$I(\vec{Q}) \propto \left|A(\vec{Q})\right|^2 \quad , \tag{1}$$

where $\vec{Q}$ is a reciprocal lattice vector, corresponding to the change of wave vector due to the scattering process. The scattering amplitude, $A(\vec{Q})$, is the Fourier transform (FT) of the thermally averaged charge density $\langle\rho(\vec{r})\rangle$. This effective density results from the averaging over two sets of variables: fast electronic motion and slow vibrational motion of nuclear centers. As a consequence, the optical contrast will be maximized for components of the density that are localized around atomic centers. Delocalized components, such as two-center contributions in a linear combination of atomic orbitals (LCAO) expansion, lead to a small optical contrast. It is thus a natural consequence of both vibrational averaging and the optical nature of scattering to impose a one-center pseudoatom expansion of the averaged density:

$$\langle\rho(\vec{r})\rangle \approx \sum_n \int \rho_n\left(\vec{r}-\vec{R}_n\right) P\left(\vec{R}_n\right) \mathrm{d}\vec{R}_n \quad , \tag{2}$$

where $P\left(\vec{R}_n\right)$ is the probability distribution function for nuclear position. This expansion leads to the following expression for the scattering amplitude:

Correspondence to: P. J. Becker
e-mail: becker@sem.ecp.fr

Contribution to the Proceedings of the 2000 Symposium on Chemical Bonding: State of the Art in Conceptual Quantum Chemistry

$$A\left(\vec{Q}\right) = \sum_n f_n\left(\vec{Q}\right) W_n\left(\vec{Q}\right) e^{i\vec{Q}\vec{R}_{n0}} \quad , \tag{3}$$

where f_n is the form factor for the pseudoatom ρ_n, W_n is the Debye–Waller factor of the nth atom and $\vec{R}_{n0}$ its equilibrium position. This model implies the existence of rigid pseudoatoms, so the density for a given geometry (denoted by $\vec{R}$) is given by

$$\rho\left(\vec{r},\vec{R}\right) = \sum_n \rho_n\left(\vec{r} - \vec{R}_n\right) \quad . \tag{4}$$

Such a rigid model would, for instance, violate the Hellman–Feynman theorem and is thus insufficient for a proper description of crystal dynamics. However, the pseudoatomic density is expanded in terms of adequate components, which are determined through a least-squares minimization procedure of the quantity

$$\sum_p \frac{\left|I_{\text{obs}}\left(\vec{Q}_p\right) - \left|A_{\text{mod}}\left(\vec{Q}_p\right)\right|^2\right|^2}{\sigma^2\left(\vec{Q}_p\right)} \quad , \tag{5}$$

$\sigma^2\left(\vec{Q}_p\right)$ being the estimated standard deviation for the pth observation. In that sense, it means that Eq. (2) or (4) is the best description of a dynamic density in terms of rigid pseudoatoms. This may constitute a reasonable definition of atoms in crystals as seen by a scattering experiment. However, of course, the relaxation of those atoms, induced by vibrations, is totally neglected [6]. Response to external forces cannot be understood on the basis of such a rigid decomposition.

From Eq. (4) it is possible to compare pseudoatoms for atoms of a given nature in similar environments and thus to estimate transferability [7]. When considering Coulombic effects between different molecular units, it often turns out that the use of transferable pseudoatoms is satisfactory [8]. This means that the difference between a density constructed from transferable fragments (coming from a data bank) and the true density is at most of the order of $0.05\text{e}\text{Å}^{-3}$, which is the usual experimental limit.

However, when looking at short distance effects, such as conformational energy changes due to torsional motions around specific bonds in polypeptides or other flexible molecules, the role of small distortions of the charge density from transferability seems essential [9]. In other words, the charge density model implied by expansions such as Eq. (4) is not sufficient for a full understanding of bonding and cohesive features in molecules or solids. One can also say that, owing to the quasitransferability of the charge density among similar environments, the energetic behavior depends not only on the charge density itself, but also on its derivatives, gradients. This is a further confirmation of the importance of the pioneering work of Bader [10] relating the topological features of the charge density to the bonding and reactivity indices in molecules.

Topological analysis has been extended to experimental densities, based again on Eq. (4), following a first study on L-alanine [11]. Such a fitted density does not fulfill the necessary requirements insuring the validity of Bader's original formulation. The fact that fitted topological features grossly follow expected trends from theoretical studies is certainly encouraging, but any strong conclusions may still be hazardous.

Consider the usual LCAO description of the density:

$$\rho = \sum_{m,n} P_{mn}\phi_m\left(\vec{r} - \vec{R}_m\right)\phi_n\left(\vec{r} - \vec{R}_n\right) \tag{6}$$

(several AOs may indeed be centered on the same nucleus). Chemical bonding is generally described through two main effects: the shape of effective AOs and the amount of delocalization between those atoms. Roughly speaking, analysis of diffraction experiments provides fairly good information concerning the symmetry of important AOs and the effective screening constants for valence orbitals. However, the two-center terms in Eq. (6), which have an effect on both electron delocalization and effective charge transfer, are only accessed through the sum of their projections over specific atomic centers. It is thus impossible to distinguish between the two mechanisms by an analysis of only the charge density. Moreover, no rigorous method exists for thermally averaging two-center terms.

2 Compton scattering and momentum density

Being an incoherent process, Compton scattering got a revival with the advent of high-intensity synchrotron radiation. This leads to the observation of directional Compton profiles (DCPs). If the 3D momentum density is denoted as $n(\vec{p})$, the DCP in the scattering direction denoted as $\vec{u}$ is the projection of the 3D density onto the direction $\vec{u}$:

$$J(q,\vec{u}) = \int\int\int n(\vec{p})\delta(q - \vec{p}.\vec{u})\mathrm{d}\vec{p} \quad . \tag{7}$$

DCPs can be measured in the principal crystallographic directions [12]. The present resolution is about 0.15 au in momentum, q, and can even be improved in some cases. Resolution is an essential factor if one wishes to retrieve chemical information from DCPs, since the contribution from valence electrons is limited to a few atomic units. A typical Compton profile is shown in Fig. 1 for MgO [13].

Current practice consists of reconstructing the 3D momentum density from a finite number of profiles, by use of a spherical harmonic expansion for $n(\vec{p})$. Numerical reconstruction, initiated by Hansen [14], is widely used, and is model free. However, we observed some systematic bias at low and large momentum, owing to the numerical nature of the method. Thus, we recently implemented an analytical procedure for reconstruction of $n(\vec{p})$, based on a Gaussian expansion of each symmetry component [15]. Namely, one assumes the following separation among momentum transfer and directional effects,

$$\vec{J}(q,\vec{u}) = \sum_l g_l(q)h_l(\vec{u}) \quad , \tag{8}$$

where $h_l(\vec{u})$ is the lattice harmonic of order l and $g_l(q)$ is expanded as a sum of Gaussian-type orbital derivatives, in such a way that the reconstructed momentum density is expressed by a simple Gaussian contraction.

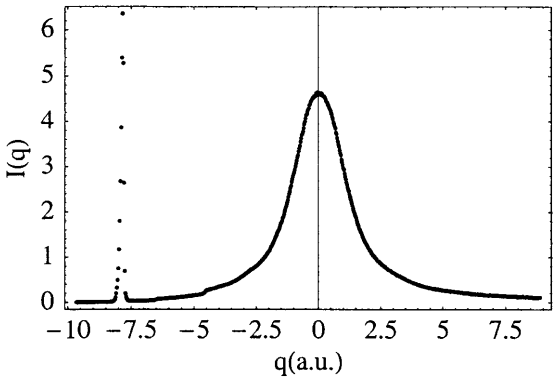

Fig. 1. Inelastic scattering spectrum in the limit of large momentum transfer. The scattering vector is aligned with the (100) direction. The Compton profile is the broad peak centered about the 0 au position. The elastic contribution is the narrow peak at −7.9 au

Tests based on ab initio calculations show the good reproducibility of our method at large momentum: for instance, kinetic energy can be adequately predicted from reconstructed density. Indeed, there is no unique way to predict a 3D function from a finite set of 1D projections: as a consequence, the 3D momentum density is not directly accessible from an experiment.

Let us recall that momentum density is the FT of the so-called autocorrelation function of the first-order density matrix:

$$n(\vec{p}) = \int B(\vec{t}) e^{i\vec{p}.\vec{t}} d\vec{t} \ , \tag{9}$$

where

$$B(\vec{t}) = \int \Gamma_1(\vec{r}+\vec{t},\vec{r}) d\vec{r} \ , \tag{10}$$

and Γ_1 is the first-order density matrix.

In terms of the natural expansion of the density matrix:

$$B(\vec{t}) = \sum n_i \int \psi_i^*(\vec{r}+\vec{t})\psi_i(\vec{r}) d\vec{r} \ , \tag{11}$$

Owing to obvious mathematical properties, a given DCP is just the 1D FT of the autocorrelation function along the direction $\vec{u}$:

$$B(t\vec{u}) = (2\pi)^{-1} \int_{-\infty}^{+\infty} J(q,\vec{u}) e^{itq} dq \ . \tag{12}$$

Therefore, momentum density conveys some information about the phase variation of the wavefunction. For comparison, we recall also that the Bragg diffracted intensity is the FT of the autocorrelation function of the charge density, the so-called Patterson function. From Eqs. (1) and (2):

$$I(\vec{Q}) = \int P(\vec{t}) e^{i\vec{Q}.\vec{t}} d\vec{t} \ .$$

$$P(\vec{t}) = \int \rho(\vec{r}+\vec{t})\rho(\vec{r}) d\vec{r} \ . \tag{13}$$

Any information about the phase of the wavefunction is thus lost in a diffraction experiment.

In a crystal, we have shown the following property [16] for a filled band system. Let $P_{m0,n\vec{L}}$ be the usual population matrix element relating two orbitals, where $(n\vec{L})$ refers to the AO of type n in unit cell $\vec{L}$. In a band structure formulation, if $\vec{k}$ denotes a wave vector in the Brillouin zone (BZ), the relevant population matrix for wave vector $\vec{k}$ is written as

$$P_{mn}(\vec{k}) = \sum_{\vec{L}} P_{m0,n\vec{L}} e^{i\vec{k}.\vec{L}} \ , \tag{14}$$

this population matrix being periodic in the reciprocal space: $P_{mn}(\vec{k}+\vec{Q}) = P_{mn}(\vec{k})$. Then, one obtains for the 3D momentum density:

$$n(\vec{p}) = \sum_{m,n} P_{mn}(\vec{p})\sigma_{mn}(\vec{p}) \tag{15}$$

$$\sigma_{mn}(\vec{p}) = \chi_m^*(\vec{p})\chi_n(\vec{p}) e^{-i\vec{p}.\vec{d}_{mn}} \ . \tag{16}$$

$\vec{d}_{mn}$ is simply the distance between two atomic centers within the unit cell. In this picture, $\vec{p}$ is identified with the wave vector of the electron within the band. Equation (16) shows a very direct connection between momentum density and the structure of the one-particle density matrix. Extension to nonfilled bands is easy, through the introduction of an occupation function within the BZ.

Structural effects only appear via the phase term involving interatomic vectors in Eq. (16). As a consequence, Compton experiments are not sensitive to lattice modes of vibration. The small effect of optic modes has not yet been quantitatively identified. At present, the Compton experiment is considered as vibration free.

For comparison, the equivalent expression for the diffraction amplitude would be

$$A(\vec{Q}) = \sum_{mn} \left[W_m(\vec{Q})W_n(\vec{Q})\right]^{\frac{1}{2}} \int_{\mathrm{BZ}} d\vec{k} P_{mn}(\vec{k})\chi_m(\vec{k}+\vec{Q}) \times e^{-i(\vec{k}+\vec{Q})\vec{R}_m}\chi_n^*(\vec{k}) e^{i\vec{k}\vec{R}_n} \ , \tag{17}$$

which implies an integration over the whole BZ, leading to a rather indirect connection with the band structure mechanism.

Thus, the collective behavior of electrons in extended solids seems to be more directly observable from an analysis of momentum density than from a diffraction experiment. *A contrario*, from Eq. (16), we observe that all one-center contributions are superimposed in the expression of momentum density, leading to the impossibility for any structural differentiation. To our understanding, this is the origin of the complementarity between the two investigations on a given compound.

3 First refinement in momentum space: LiH

We performed the first extensive refinement on Compton profiles for LiH [16]. From Eq. (16) it occurs that an explicit model for the population matrix is necessary at each wave vector in the BZ.

Measurements can only be performed for electron momentum less than a few atomic units: only core electrons contribute to large momentum transfer. As a consequence, one must assume a total separability between core and valence densities. Core density is calculated from free atoms (Li $1s^2$ in the present case). One defines the valence density as

$$n_{\mathrm{v}}(\vec{p}) = n(\vec{p}) - n_{\mathrm{core}}(p) \ . \tag{18}$$

Owing to the strong ionic character of this compound, we built the valence electron wavefunctions as follows. We consider a cluster centered on the anion, and surrounded by six first-neighbor cations and write the wavefunction for this cluster as

$$\phi(\vec{r}) = N\left\{\varphi_{\mathrm{H}}(\vec{r}) + \frac{\lambda}{\sqrt{6(1+S_{\mathrm{LiLi}})}}\left[\sum_{j=1}^{6}\varphi_{\mathrm{Li}}(\vec{r}-\vec{R}_j)\right]\right\} \ , \tag{19}$$

The Li orbitals are $2s$ type (adjunction of hybridization appeared to be insignificant). We then construct Bloch orbitals as

$$\psi\left(\vec{k},\vec{r}\right) = \frac{1}{\sqrt{NS\left(\vec{k}\right)}}\sum_{\vec{L}}\phi\left(\vec{r}-\vec{L}\right)\mathrm{e}^{i\vec{k}.\vec{L}} \ ,$$

$$S\left(\vec{k}\right) = \sum_{\vec{L}}\left\langle\phi(\vec{r})\middle|\phi\left(\vec{r}-\vec{L}\right)\right\rangle\mathrm{e}^{i\vec{k}.\vec{L}} \ , \tag{20}$$

with full account for overlap between very diffuse anion orbitals. This model wavefunction is approximate, but should reveal the mechanism for incomplete charge transfer. AOs are approximated by Slater-type orbitals (STOs), so the adjustable parameters are the effective screening constants of H and Li on the one hand and the λ coupling coefficient on the other hand. The 3D momentum density was reconstructed numerically from 12 DCPs, and a least-squares refinement was performed on $n_{\mathrm{v}}(\vec{p})$, taking estimated errors into account. Notice that the case $\lambda = 0$ corresponds to the fully ionic model for the crystal. The relevance of the refinement procedure is mostly revealed on comparison between fitted and observed DCPs. It turns out that the most sensitive functions are the so-called Compton anisotropies, defined as the difference between DCPs in two different directions. $(J_{100} - J_{110})$ is shown in Fig. 2: it shows the difference of behavior of electrons among the two basic crystallographic directions of Li–H and H–H first contacts. We observe that a three-parameter fit is as good as a full ab initio CRYSTAL95 calculation [17]. The fitted parameters are $\zeta_{\mathrm{H}} = 0.74(1)$, $\zeta_{\mathrm{Li}} = 0.59(1)$, $\lambda = -0.32(2)$.

The effective screening constants are in close agreement with predicted values from quantum screening rules. The effective covalency of the bonds is about 10%.

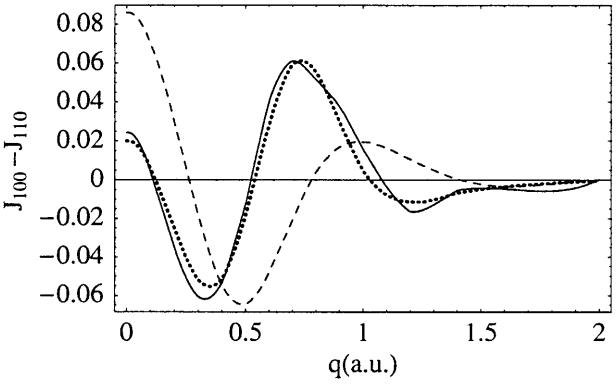

Fig. 2. Compton relative anisotropy defined as the difference between directional Compton profiles in the (100) and the (110) directions. Experiments: *solid line*. Refined model with 10% effective covalency: *dotted line*. Refined model without covalency: *dashed line*

We also display the anisotropy from a refinement where the crystal is assumed to be purely ionic ($\lambda = 0$). The discrepancy is striking, both for the magnitude and the phase of the anisotropy.

This analysis clearly shows that anisotropic features in momentum space are highly sensitive to the interatomic coupling of valence wavefunctions.

4 MgO: a combined study in real and momentum space

Structure factors of MgO have been continuously measured. In particular, a recent experiment was performed using convergent beam electron diffraction [18] in order to measure accurate values for the low-angle structure factors, which are the most sensitive to cohesive forces; the limit in $\sin\theta/\lambda$ for those measurements is 0.5 $\mathrm{\AA}^{-1}$. Higher scattering angle data, mostly insensitive to valence electrons, but essential for the estimate of Debye–Waller factors, are taken from Ref [19]. Owing to some ambiguities in the discussion, the analysis was reconsidered by Gillet and Cortona [20]. As usual, the one-center expansion is assumed to be

$$F(hkl) = 4\left[f_+W_+ + (-1)^{h+k+l}f_-W_-\right] \ . \tag{21}$$

Besides the usual type of pseudoatom description (including rescaling of effective valence densities, adjustable charge transfer), the following decomposition is proposed for cation and anion form factors:

$$f_+ = f_{\mathrm{Mg}^{2+}}(Q) + \frac{2-q}{2}f_{\mathrm{Mg},3s}(Q) \ ,$$

$$f_- = f_{\mathrm{O}^{2-}}(Q) + (q-2)\delta f(Q) + \varphi(Q)K_4\left(\hat{Q}\right) \ . \tag{22}$$

A DFT calculation on the solid was performed by the method proposed by Cortona [21], in which the density is constrained to be the sum of ionic components of spherical symmetry. This method provides optimal ionic densities, or conversely ionic form factors $f_{\mathrm{Mg}^{2+}}, f_{\mathrm{O}^{2-}}$: notice that this method leads to accurate cohesive energies, lattice parameters and bulk moduli in various

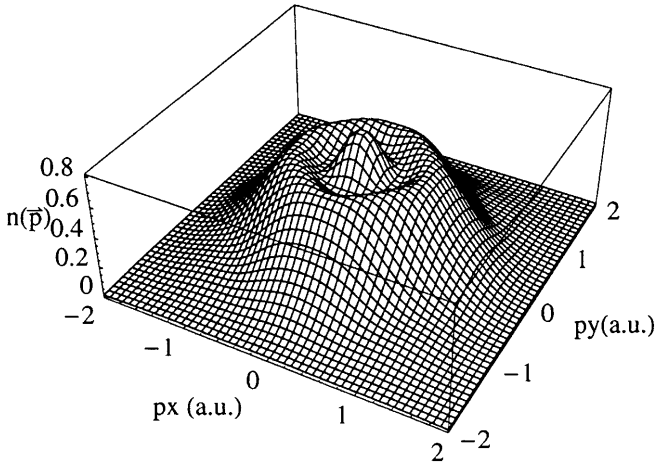

Fig. 3. Reconstructed electron momentum density using the analytical method

series of ionic solids. One unique advantage of this method is the possibility to define anionic density. In order to improve the fit to observed structure factors, additive contributions are added. First, the charge transfer is assumed to be incomplete, which leads to a partial occupation of the 3*s* state for the cation. Conversely, the modification in the anion is modeled by a Slater-type function, the FT of which is δf. Finally, a nonspherical contribution for the anion is included, limited to the first fourth-order cubic harmonic component (also represented by a STO). Such a simple model, with only five parameters, leads to a fair agreement with experimental structure factors. The nonspherical component has a very small effect on the structure factors, though it significantly affects the global reliability of the fit. q, the effective charge of the anion, is between 1.8 and 2 for various refinements. The analysis leads to a fair and stable description of the effect of crystal forces on the effective oxygen density. Nevertheless, it turns out to be impossible to decide among several fits, which all lead to a prediction of structure factors better than 1%. As a conclusion, it turns out that even precise knowledge of the charge density is not sufficient for understanding the nature of interactions in a crystal such as MgO.

Parallel to this study, we performed a precise measurement of DCPs at the European Synchrotron Research Facility (D15B), along eight different crystallographic directions [13, 22]. The 3D momentum density was reconstructed through our analytical procedure, as described previously. The necessary strategy for refinement is more complex than for LiH, since four valence bands are populated in this crystal. We kept the idea of representing the solid as a periodic array of {O,6Mg} clusters, each cluster containing eight valence electrons. The four wavefunctions of the cluster are:

$$\phi_s = N_s\left(\varphi_{s,\mathrm{O}} + \lambda_s N'_s \sum_{j=-3, j\neq 0}^{3} \varphi^j_{s,\mathrm{Mg}}\right) ,$$

$$\phi_{p_j} = N_p\left[\varphi_{p_j,\mathrm{O}} + \lambda_p N'_p\left(\varphi^j_{s,\mathrm{Mg}} - \varphi^{-j}_{s,\mathrm{Mg}}\right)\right],\ j = x,y,z \quad (23)$$

where $\varphi^{\pm j}_{s,\mathrm{Mg}}$ stands for the *s*-type orbital of the Mg atom centered at $\pm\frac{a}{2}\vec{e}_j$. The function centered on the oxygen (taken at the origin) can be s or p type. Four Bloch functions can be defined from Eq. (23), according to the procedure of Eq. (19). If we call $\eta_i(\vec{p})$ the FT of each of the four cluster wavefunctions, the valence momentum density is written as

$$n_{\mathrm{v}}(\vec{p}) = \sum_{i,j=1}^{4} \Sigma^{-1}(\vec{p})_{ij}\eta^*_i(\vec{p})\eta_j(\vec{p}) \ , \quad (24)$$

where $\Sigma^{-1}(\vec{p})$ is the inverse overlap matrix among the four Bloch functions.

Owing to an expected weak covalency together with a great similarity of Debye–Waller factors for the two ions [18], the following expression for the structure factors could be used:

$$F(hkl) = 4\left\{f_+ W_+ + (-1)^{h+k+l} f_- W_-\right\} \ , \quad (25)$$

$$f_+ = f_{\mathrm{Mg}^{2+}}(Q) \ ,$$

$$f_- = f_{\mathrm{O},1s}(Q) + \int |\phi_s|^2 \mathrm{e}^{i\vec{Q}.\vec{r}}\mathrm{d}\vec{r} + \sum_{j=1,3}\int \left|\phi_{p_j}\right|^2 \mathrm{e}^{i\vec{Q}.\vec{r}}\mathrm{d}\vec{r} \ . \quad (26)$$

The model given by Eq. (23) uses ionic type functions from the previously cited work on MgO [20]. The refined parameters include scaling and mixing factors [13, 23] and result from a joint refinement of low-order structure factors and the three main DCPs are summarized in Figs. 4 and 5. They show, for the first time, the

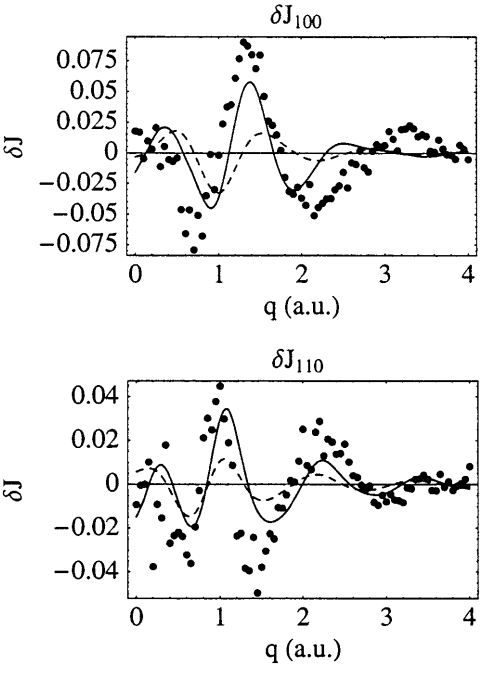

Fig. 4. Comparison of absolute anisotropies for chemically important directions. European Synchrotron Research Facility measurements: *dots*. Ionic model ($R_{\mathrm{j}} = 1.6\%$): *dashed line*. Results from joint refinement ($\lambda_s = 10^{-2}$; $\lambda_p = 10^{-1}$; $R_j = 1.3\%$): *solid line*

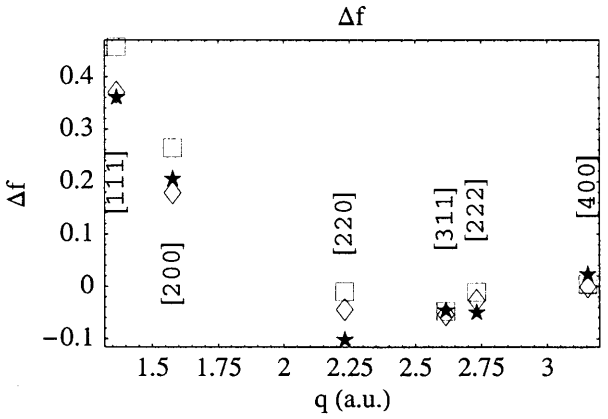

Fig. 5. Comparison of Δf defined by $\Delta f(h,k,l) = (-1)^{h+k+l}\left[F(h,k,l) - 4f_{Mg^{2+}}(h,k,l) - (-1)^{h+k+l}4f_O(h,k,l)\right]/4$. Measurement [18]: *stars*. Ionic model resulting from density functional theory ($R_F = 0.74\%$): *squares*. Results from the joint refinement ($\kappa_{O,2s} = 0.998$; $\kappa_{O,2p} = 1.028$; $\kappa_{Mg,3s} = 1$; $R_F = 0.35\%$): *diamonds*

possibility to refine valence wavefunctions from combined structure factors and DCPs, and the decoupling between local and delocalized effects in electron behavior.

5 Correlation in ionic crystals?

As discussed earlier, subtleties of chemical bonding are mostly revealed via the anisotropy of the momentum density. One advantage related to that observation is the fact that most inadequacies in the measurement process will cancel out when considering those anisotropies of Compton profiles: as a consequence, even small fluctuations of that sort become highly significant.

Let us nevertheless consider in more detail the comparison between the experimental and the theoretical isotropic part of the total DCPs. Both for LiH and MgO, we observe a systematic difference between experimental and CRYSTAL95 Hartree–Fock (HF) SCF profiles, which is similar for all directions, and can therefore be considered as isotropic in nature [13]. The average difference is shown for both compounds in Figs. 6 and 7 (dotted lines); it is defined as $\Delta J_{exp}(q) = \langle J_{exp}(q)\rangle - \langle J_{HF}(q)\rangle$, where the directional average is taken from principal directional profiles, together with uncertainties. For LiH, the experimental profile is lower than the HF profile at low momentum and higher in the case of MgO. In other words, valence electrons seem to be more localized than predicted at the HF level for LiH and are more delocalized for MgO.

We first thought that this discrepancy was related to systematic errors in the measurements. For MgO, by analyzing previous measurements by Aikala et al. [24], we found a similar difference. Changing the basis set for both LiH and MgO led to unaltered conclusions. It is thus not unreasonable to quote some physical reasons for those systematic differences. Therefore, we consider the possibility for electron correlation effects to be significant in those compounds, and more interesting to be observable through a quantitative analysis of momentum density.

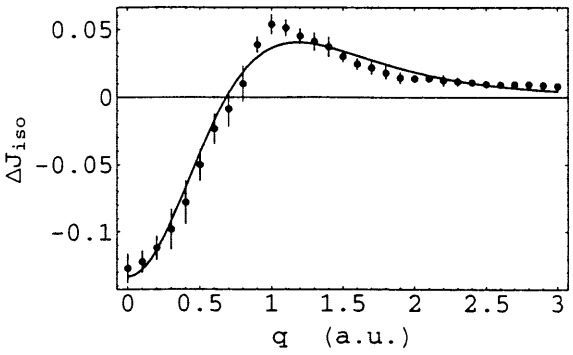

Fig. 6. Refinement of isotropic difference between experimental and Hartree–Fock (*HF*) Compton profile of LiH. Experiment: *dotted line with error bars*. Model: *full line*

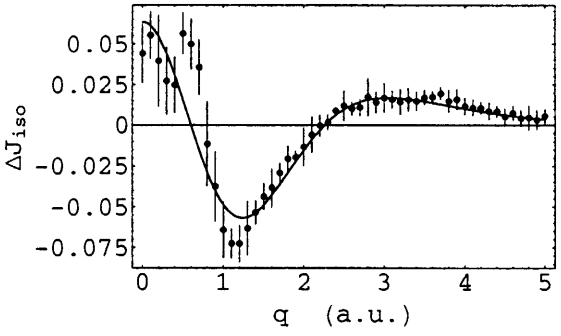

Fig. 7. Refinement of isotropic difference between experimental and HF Compton profile of MgO. Experiment: *dotted line with error bars*. Model: *full line*

Correlation effects should be significant for valence electrons in anions that are confined to a finite region of space, as compared with free ions. We have undertaken a full analysis of this effect by calculating correlated wavefunctions for clusters that mimic the crystal behavior. Meanwhile, we want to propose a simple empirical mechanism to account for correlation.

First consider LiH, and more specifically the pair of valence electrons around the hydrogen ion. The correlation mechanism can result in a double effect. The repulsion between the two electrons will expel one electron further from the nucleus, and as a result the other will feel a reduced screening compared with the uncorrelated situation. Therefore, starting from a doubly occupied STO,

$$\psi_0(1,2) = N e^{-\zeta(r_1+r_2)} \quad , \tag{27}$$

we propose the following approximation for the correlated pair:

$$\psi(1,2) = N'\left(e^{-\alpha r_1}e^{-\beta r_2} + e^{-\alpha r_2}e^{-\beta r_1}\right)(1 + \eta \vec{r}_1.\vec{r}_2) \quad . \tag{28}$$

The angular correlation is accounted for by the term $\eta \vec{r}_1.\vec{r}_2$, though radial correlation occurs via the unbalance of the effective nuclear charges for the two electrons. This simple model allows separate study of both radial and angular correlation. This was further validated by a variational calculation on two electron ions, and led to results that are in fair agreement with

ab initio calculations (the correlation energy obtained for the free hydrogen ions is about 65% of the exact one). The model difference Compton profiles $\Delta J(q) = J(q) - J_0(q)$ were derived from Eqs. (26), (27) and (28) and then refined with respect to experimental isotropic difference $\Delta J_{\exp}(q) = \langle J_{\exp}(q) \rangle - \langle J_{\mathrm{HF}}(q) \rangle$. The constraint $\zeta = \frac{1}{2}(\alpha + \beta)$ was applied. The result of the refinement is shown in Fig. 6 (full line). The refined parameters are $\alpha = 1.46$ (± 0.06) and $\beta = 1.64$ (± 0.06). η turned out to be insignificant and was set to 0. $J_{\exp}(q)$ is shifted towards momenta comparable to those of core electrons of lithium. This shows that, for a further analysis, the environment of the anion is to be considered explicitly, in the same way as discussed in Sect. 4. The extension of such clusters to incorporate correlation effects is under study. The agreement between the experimental difference and our model is very satisfactory, but led to an overestimate of the kinetic energy; $\Delta \mathrm{KE}_{\exp} = \mathrm{KE}_{\exp} - \mathrm{KE}_{\mathrm{HF}}$ being estimated from $\Delta J(q)$.

For the oxygen ion in MgO, the problem is more complex since we must at least consider eight electrons, and thus four pairs undergoing exchange. Nevertheless, if we consider an average effect for each pair (the four being equivalent), it is still possible to write the effective pair wavefunctions as

$$\psi_0(1,2) = N r_1 r_2 \mathrm{e}^{-\zeta(r_1 + r_2)} \ , \tag{29}$$

$$\psi(1,2) = N' r_1 r_2 \left(\mathrm{e}^{-\alpha r_1}\mathrm{e}^{-\beta r_2} + \mathrm{e}^{-\alpha r_2}\mathrm{e}^{-\beta r_1}\right)(1 + \eta \cos\, \theta_{12}) \ . \tag{30}$$

The refinement of $\Delta J(q) = J(q) - J_0(q)$, derived from such functions is shown in Fig. 7 (full line).

The parameters obtained are $\alpha = 4.15(\pm 0.12)$, $\beta = 2.78$ (± 0.12) and $\eta = -1.53$ (± 0.23). Angular correlation is significant in that case. For ions described by *s*-type orbitals, η is generally quite smaller (around -0.1) and a proper interpretation should include $2p$ orbitals explicitly. The mutual screening of electrons appears to be more pronounced than in the LiH case but is partially compensated by the angular term, so the resulting effect for MgO is proportionally smaller in magnitude than for LiH. We further observe that $\Delta J_{\exp}(q)$ is positive at both low and high momenta; this phenomenon is also to be observed for effective ions, when comparing correlated and uncorrelated profiles. The effect of correlation on kinetic energy, estimated from this simple model, turns out to be adequate in this case of MgO.

Subsequently, correlation effects for valence electrons might be understood as being mainly intraanionic in the case of MgO, whereas they lead to a slight charge transfer from H^- to Li^+ in the former case.

6 Conclusion

Even though our model is too crude, it is plausible that accurate measurements of Compton profiles, analyzed through a wavefunction refinement, together with analysis of structure factors, may lead to very fruitful information concerning chemical bonding.

1. Structure factors are highly sensitive to the shape and nature of important AO contributions to form the solid.
2. Compton profiles can lead to a nice description of the coupling among adjacent atoms.
3. Finally, after a precise refinement in both spaces, remaining discrepancies can be analyzed in terms of possible mechanisms for correlation effects in ions or solids.

We feel that extending such types of analysis to more covalent or metallic solids might be helpful for a better management of cohesive forces: another interesting situation being that of molecular solids where Compton scattering could lead to an improved understanding of intermolecular forces [25], such as for hydrogen bonding, where a recent experiment [26] on ice led to much controversy [27]. The experimental anisotropy of the Compton profiles was interpreted as the signature of a hydrogen-bond effect [25]. This conclusion was then contradicted by a theoretical study on a dimer of noninteracting water molecules, where just Pauli repulsion was incorporated [27] and the authors obtained qualitatively similar features to the experimental observation and concluded that this experiment could not provide evidence for cohesive forces in ice. We believe that the conclusions cannot be so drastic. First of all, Pauli repulsion is part of cohesive interaction, and another model, which incorporates both repulsive and attractive contributions (we have undertaken such a study), has to be used. Coming back to the effect of repulsion between closed shells, let us end with a very simple model. Assume two doubly occupied equivalent orbitals, ϕ_1, ϕ_2, whose centers are distant by $\vec{R}$. The one-particle density matrix is written as

$$\gamma(\vec{r},\vec{r}') = \frac{2}{(1-S^2)}\left[\phi_1(\vec{r})\phi_1(\vec{r}') + \phi_2(\vec{r})\phi_2(\vec{r}') - S\phi_1(\vec{r})\phi_2(\vec{r}') - S\phi_2(\vec{r})\phi_1(\vec{r}')\right] \ . \tag{31}$$

The effect on the charge density is of second order in overlap,

$$\rho(\vec{r}) = \frac{2}{(1-S^2)}\left[\phi^2(\vec{r}) + \phi^2\left(\vec{r} - \vec{R}\right) - 2S\phi(\vec{r})\phi\left(\vec{r} - \vec{R}\right)\right] \ , \tag{32}$$

though it is of first order for momentum density:

$$n(\vec{p}) = \frac{4\chi^2(\vec{p})}{(1-S^2)}\left(1 - S\mathrm{e}^{i\vec{p},\vec{R}}\right) \ . \tag{33}$$

Therefore, the momentum density is, in principle, more adapted to intermolecular effects than charge density. The controversy about ice needs further discussion.

References

1. Coppens P (1997) X-ray charge densities and chemical bonding. Oxford University Press, Oxford
2. Tsirelson VG, Ozerov RP (1996) Electron density and bonding in crystals. Institute of Physics, Bristol
3. Porcher F, Souhassou M, Dusausoy Y, Lecomte C (1999) Eur J Mineral 11: 333

4. Lecomte C (1999) Implications of molecular and material structure for new technologies. Kluwer, Dordrecht, p 23
5. Pressprich M, White MA, Vekhter Y, Coppens P (1994) J Am Chem Soc 116: 5233
6. Becker P (ed) (1980) Electron and magnetization distributions in solids, Plenum, New York
7. Pichon-Pesme V, Lecomte C, Lachekar H (1995) J Phys Chem 99: 6242
8. Becker P, Bec E (1996) Chem Phys Lett 260: 319
9. Bec E (1998) Thesis. Ecole Centrale, Paris
10. Bader RFW (1994) Atoms in molecules: a quantum theory. Clarendon, Oxford
11. Lawrence JL (1973) Acta Crystallogr A 29: 94
12. Cooper MJ (1997) Radiat Phys Chem 50: 63
13. Fluteaux C (1999) Thesis. Ecole Centrale, Paris
14. Hansen NK (1986) Hahn Meitner Institute report, Berlin
15. Gillet JM, Fluteaux C, Becker P (1999) Phys Rev B 60: 2345
16. Gillet JM, Becker P, Loupias G (1995) Acta Crystallogr A 51: 405
17. Dovesi R, Saunders VR, Roetti C, Causa M, Harrison N, Orlando R (1996) 17-CRYSTAL95 user's manual. Torino
18. Zuo JM, O'Keeffe M, Rez P, Spence JCH (1997) Phys Rev Lett 78: 4777
19. Destro R, Bianchi R, Gatti C, Merati F (1991) Chem Phys Lett 186: 7
20. Gillet JM, Cortona P (1999) Phys Rev B 60: 8569
21. Cortona P (1992) Phys Rev B 46: 2008
22. Fluteaux C, Gillet JM, Becker P (2000) J Phys Chem Solids 61: 369
23. Beckers O (1997) Thesis. Ecole Centrale, Paris
24. Aikala O, Paakari T, Manninen S (1982) Acta Crystallogr A 38: 155
25. Belemlilga D, Gillet JM, Becker P (1999) Acta Crystallogr B 55: 192
26. Isaacs ED, Shukla A, Platzmann PM, Hamann DR, Barbiellini B, Tulk CA (1999) Phys Rev Lett 82: 600
27. Ghanty TK, Staroverov VN, Koren PR, Davidson ER (2000) J Am Chem Soc 122: 1210